Wu et al. Journal of Nanobiotechnology (2015) 13:35
DOI 10.1186/s12951-015-0094-4

JOURNAL OF NANOBIOTECHNOLOGY

RESEARCH Open Access

Nanodiamonds protect skin from ultraviolet B-induced damage in mice

Meng-Si Wu[1,2], Der-Shan Sun[2,7], Yu-Chung Lin[4], Chia-Liang Cheng[4,5], Shih-Che Hung[7], Po-Kong Chen[2], Jen-Hung Yang[6,7,8] and Hsin-Hou Chang[2,3,5,7*]

Abstract

Background: Solar ultraviolet (UV) radiation causes various deleterious effects, and UV blockage is recommended for avoiding sunburn. Nanosized titanium dioxide and zinc oxide offer effective protection and enhance cosmetic appearance but entail health concerns regarding their photocatalytic activity, which generates reactive oxygen species. These concerns are absent in nanodiamonds (NDs). Among the UV wavelengths in sunlight, UVB irradiation primarily threatens human health.

Results: The efficacy and safety of NDs in UVB protection were evaluated using cell cultures and mouse models. We determined that 2 mg/cm^2 of NDs efficiently reduced over 95% of UVB radiation. Direct UVB exposure caused cell death of cultured keratinocyte, fibroblasts and skin damage in mice. By contrast, ND-shielding significantly protected the aforementioned pathogenic alterations in both cell cultures and mouse models.

Conclusions: NDs are feasible and safe materials for preventing UVB-induced skin damage.

Keywords: Nanodiamonds, Ultraviolet, Sunburn, Sunscreen

Background

All life forms on Earth are greatly influenced by solar energy (electromagnetic radiation), which includes ultraviolet (UV; 200–400 nm), visible (400–700 nm), and infrared radiation. UV radiation is classified as UVC (200–290 nm), UVB (290–320 nm), and UVA (320–400 nm), and these high-energy radiation can damage cells [1]. The ozone layer absorbs almost all UVC and a part of the UVB wavelengths, thus protecting against severe UV damage. UVA is less harmful, and UVB is the primary threat to human health, causing acute sunburn, photoaging, immunosuppression, and skin cancers [2,3]. Even brief exposure to UV can induce DNA damage, such as pyrimidine dimers [cyclobutane pyrimidine dimer and the (6–4) photoproducts], which can be carcinogenic in the absence of adequate reparative processes [4]. Moreover, in 1985, Farman et al. reported springtime ozone depletion (ozone hole) over the Antarctic region [5]. The World Health Organization (WHO) developed the UV Index (UVI) to quantify UV radiation; its daily forecasts are currently used in several countries for people to adopt adequate protective measures [6,7].

Using sunscreens to block UV and avoiding excessive solar exposure are recommended for preventing sunburns [8]. Macro-sized titanium dioxide (TiO_2) and zinc oxide (ZnO) are conventional and safe sunscreen ingredients but have the disadvantages of uneven coverage and an opaque white appearance [9]. By contrast, nanosized TiO_2 and ZnO provide more effective protection and acceptable cosmetic appearance and have been widely used in commercial sunscreens since the late 1990s [10]. However, health concerns regarding systemic absorption and reactive oxygen species (ROS) gradually increased [11]. Studies have shown no increased penetration of these nanoparticles (NPs) in intact skin [12,13], but it remains a concern in sunburned skin [14]. Moreover, minor contamination with anatase crystals of rutile nanosized TiO_2 can elicit photocatalysis and induce cellular damage [15].

Currently, nanodiamonds (NDs) are widely investigated nanomaterials. Because of their nontoxicity and biocompatibility, they are especially suitable for biomedical

* Correspondence: hhchang@mail.tcu.edu.tw
[2]Department of Molecular Biology and Human Genetics, Tzu-Chi University, No. 701 Sec. 3, Chung-Yang Rd, Hualien City, Hualien County 970, Taiwan
[3]Research Center of Nanobiomedical Science, Tzu-Chi University, No. 701 Sec. 3, Chung-Yang Rd, Hualien City, Hualien County 970, Taiwan
Full list of author information is available at the end of the article

applications such as drug delivery and bioimaging [16]. In addition, NDs attenuate UV radiation through absorption and scattering, a phenomena dependent on factors such as ND particle size and nitrogen defects [17]. Although NDs are theoretical sunscreen candidates according to absorption spectral studies, few studies have assessed their practical protective effects. Therefore, we investigate the efficiency and safety of NDs as a UV filter in both animal and cell culture models and compare the results with those of nanosized TiO_2 and ZnO.

Results

UVB attenuation by nanosized ND-, TiO_2-, and ZnO-coated films

The UVB attenuation abilities of 5- and 100-nm NDs, nanosized TiO_2, and ZnO and the association between nanomaterial concentration and UVB intensity were tested (Figure 1A, experiment setting). All four nanomaterials significantly reduced UVB intensity to a safe range (UVI < 2, Figure 1B-E) defined by WHO [6,7] even under the extreme UVB exposure of UVI 11 (Figure 1E). At a nanomaterial concentration of 2 mg/cm^2, TiO_2, ND, and ZnO exhibited approximately 99%, 94%, and 90% of UVB-blocking efficiencies, respectively. The efficiency of TiO_2 was significantly higher than that of ZnO at all tested doses but higher than that of ND only at lower concentrations (1 and 2 mg/cm^2) (Additional file 1: Figure S1). This experiment demonstrated ND efficiency in UVB attenuation.

NDs protect cells from UVB damage

The protective efficiency of NDs was further investigated using a cell culture model. All four nanomaterials at medium–high concentrations (≥2 mg/cm^2) protected human immortalized HaCaT keratinocytes and mouse embryonic fibroblasts (MEFs) from UVB damage (Figure 2). After UVB irradiation at a UVI of 6 for 10 min, all four tested nanomaterials (ZnO, TiO_2, and 5- and 100 nm-NDs) offered considerable protection at all tested doses in HaCaT cell group, and the 100-nm NDs were the optimal materials for UVB irradiation shielding (Figure 2A, experiment setting; Figure 2B). By contrast,

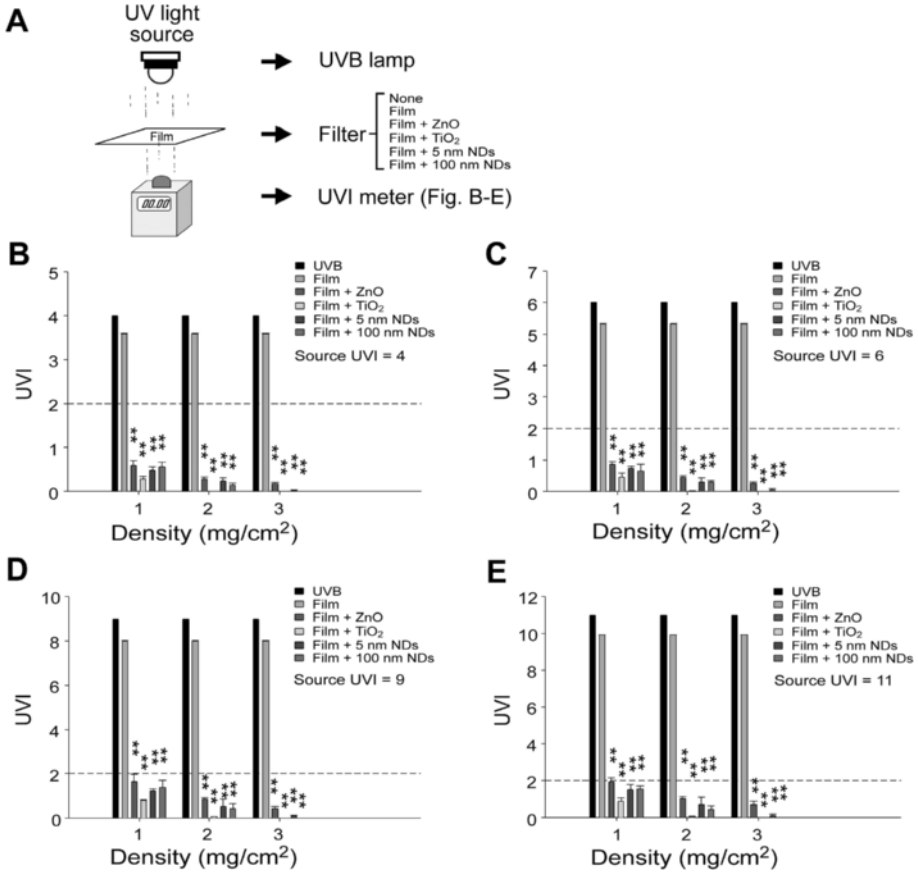

Figure 1 UVB attenuation by ND- and nanosized TiO_2- and ZnO-coated films. Experiment setting **(A)**. Detected UVB UVI levels of the tested nanomaterial films at various nanomaterial concentrations. UVB at UVIs of 4 (100 mW/m^2 UV_{Ery}) **(B)**, 6 (150 mW/m^2 UV_{Ery}) **(C)**, 9 (225 mW/m^2 UV_{Ery}) **(D)**, and 11 (275 mW/m^2 UV_{Ery}) **(E)** were analyzed. The dashed line indicates a UVI of 2 (50 mW/m^2 UV_{Ery}), and UVB below this level is considered safe **(B–E)**. n = 3, *P < 0.05, **P < 0.01. Data are mean ± SD.

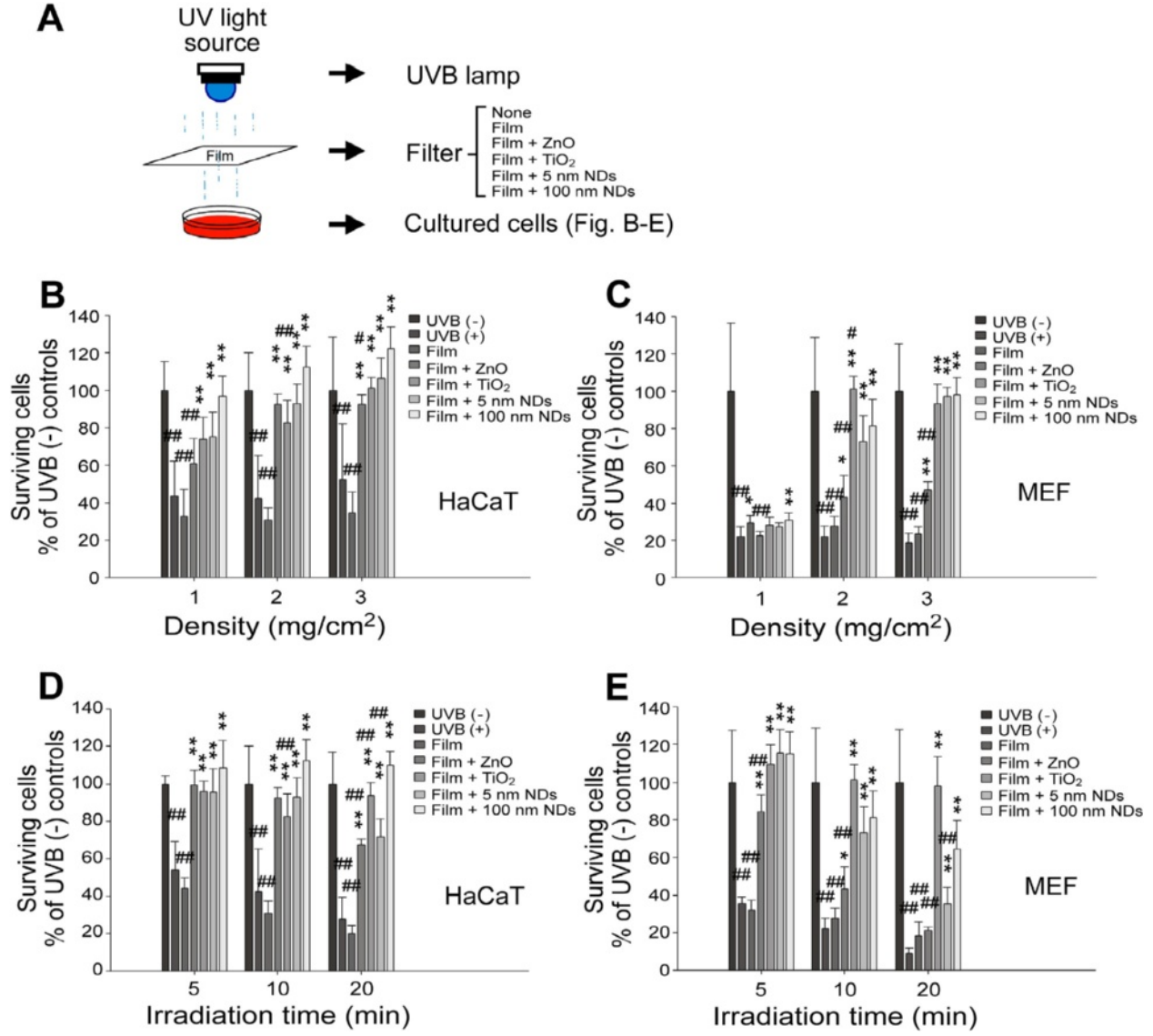

Figure 2 NDs protect cultured cells from UVB damage. Experiment setting **(A)**. Dose dependent **(B, C)** (UVI 6 for 10 min [68 mJ/cm^2] at 1, 2, and 3 mg/cm^2 density) and time-dependent **(D, E)** (UVI 6 for 5 and 10 min [34 and 68 mJ/cm^2] at 2 mg/cm^2 density) responses of nanomaterials in UVB protection of HaCaT **(B, D)** and MEF **(C, E)** cells were measured using the WST-1 assay. n = 6 (three experiments repeated twice). Groups without UVB exposure [UVB (–) control] was normalized to 100%. n = 6 (three experiments repeated twice); $^{*}P < 0.05$, $^{**}P < 0.01$, significantly better as compared with UVB (+) groups; $^{\#}P < 0.05$, $^{\#\#}P < 0.01$, significantly worse as compared with Film + 100-nm NDs" groups. Data are mean ± SD. The 10-min groups in **(D)** and **(E)** are adoptive from 2 mg/cm^2 groups in **(B)** and **(C)**, respectively.

MEFs were more sensitive to UVB under the same conditions [Figure 2B–C; UVB (+) group survival in MEFs was lower than that in HaCaT cells]. All tested materials did not offer adequate protection at low concentrations (1 mg/cm^2) (Figure 2C). The protective efficiency of all materials increased (TiO_2 > NDs > ZnO) on increasing the concentration to 2 mg/cm^2. No significant differences were observed between 5-nm and 100-nm ND groups, whose cell viability averaged 73% and 82%, respectively (Figure 2C). At 3 mg/cm^2, the cell viability of ND groups increased and did not differ significantly from that of the TiO_2 group. However, no clear improvement was noted in the ZnO group (Figure 2C). Untreated MEF cells attached normally and displayed fusiform appearance. By contrast, after direct UVB exposure with and without shielding with transparent plastic films, fewer cells attached and were surrounded by cellular debris (Additional file 1: Figure S2).

Next, the influence of irradiation time on cell viability was examined. In agreement with the dose experiments of the shielding materials, HaCaT keratinocytes displayed relatively higher resistance against UVB irradiation; at a

concentration of 2 mg/cm^2, all tested materials offered considerable protection after 5-, 10-, and 20-min UVB irradiations (Figure 2D). Because the protective efficiency of 100-nm ND was significantly higher than those of all other materials in the 20-min group (Figure 2D), it is the optimal material. By contrast, in MEF experiments, complete protection was observed only in the 5-min group; the efficiency of ZnO continued to be lower than those of the others (Figure 2E). The mechanism underlying 100-nm ND and TiO_2 being optimal for HaCaT cell and MEF survival, respectively, is unclear. A possible explanation is the differential sensitivity of these two cells types in response to wavelengths after differential UVB absorption, penetration, and emission; this mechanism is worthy of further investigation. These results collectively indicate the protective efficiency of ND against UVB irradiation. In addition, 100-nm NDs exhibit enhanced performance compared with 5-nm NDs (Figure 2D–E, 20-min group). Consequently, we focused on 100-nm NDs in the subsequent *in vivo* experiments.

NDs do not exhibit photocatalytic activity

Both ZnO and anatase form TiO_2 exhibit UV-induced photocatalytic activities [18-20], which induces ROS and damages human cells. In addition, impurity doping leads to anatase TiO_2 exhibiting photocatalytic activity under visible light irradiation [21-27]. Although rutile TiO_2 is used in cosmetic applications, minor anatase crystal contamination may elicit photocatalysis and induce cellular damage. Therefore, the photocatalytic activities of the four tested materials were analyzed using methylene blue (MB) degradation experiments. Both 5- and 10-nm NDs exhibited no obvious photocatalytic activity compared with the negative control MB group (Additional file 1: Figure S3). By contrast, rutile and anatase TiO_2 samples considerably degraded MB (Additional file 1: Figure S3; anatase TiO_2 was the positive control). These results suggested that NDs do not exhibit UVB-inducible photocatalytic activities.

NDs protect C57BL/6J mouse skin from UVB-induced inflammation

The outermost strata of normal human skin are composed of multiple layers of dead corneocytes. Because the aforementioned cell culture model may not comprehensively reflect the complexity of human skin, an animal model was designed for studying the UVB-blocking efficiency of NDs. C57BL/6J mice were subjected to 20-min UVB irradiation at a UVI of 6 daily for three consecutive days; skin damage developed from the third day. An enzyme-linked immunosorbent assay (ELISA) detected elevation of both tumor necrosis factor-α (TNF-α) and interleukin-1β (IL-1β), two proinflammatory cytokines (Figure 3A, experiment setting; Figure 3B). The preliminary analysis showed that IL-1β increased earlier than TNF-α did and peaked 24 h after the second irradiation (Additional file 1: Figure S4A–S4B). Circulating TNF-α increased abruptly 24 h after the third irradiation, with the level corresponding to the severity of skin damage (Additional file 1: Figure S4B–S4D). To prevent skin damage outside the tested area (Additional file 1: Figure S4D), aluminum foil covered the nontested regions in subsequent experiments (Figure 3A). In placebo groups, materials such as vehicle, TiO_2, and 100-nm NDs (2 mg/cm^2) applied without UVB exposure were safe. By contrast, in mice receiving the aforementioned materials under the same conditions but irradiated with UVB at a UVI of 6, those covered with TiO_2 and NDs showed only milder injuries compared with those covered with vehicle (Figure 3A-2). To further analyze the protective role of NDs in epidermal barrier functions, a dye exclusion experiment was employed, following methods modified from previous reports [28,29]. UVB irradiation damaged the epidermal barrier function of the experimental mice, thus causing higher levels of dye retention in the skin tissues (Additional file 1: Figure S5, vehicle groups). By contrast, TiO_2- and 100-nm-ND-shielded skin samples tended to maintain a relatively undamaged epidermal barrier function, as indicated by the dye retention levels, which were lower than those in vehicle-shielded control groups (Additional file 1: Figure S5). Cytokine level changes were consistent with the skin damage results. In the experiment without UVB irradiation, nanosized TiO_2 and 100-nm NDs did not induce TNF-α and IL-1β elevation (Figure 3B), suggesting that these materials are safe on mouse skin. After UVB exposure, both TNF-α and IL-1β in TiO_2 and ND groups were significantly lower than those in vehicle groups, and no differences were observed between those of TiO_2 and NDs. These results suggested that 100-nm NDs protect mouse skin from UVB damage at an efficiency comparable with that of nanosized TiO_2 (Figure 3B).

NDs ameliorate UVB-induced skin hyperplasia and leukocyte infiltration

Previous reports have indicated that hyperplasia of the strata granulosum and spinosum and increased leukocyte infiltration are involved in histological changes of UVB-irradiated skin [30,31]. In our study, considerable hyperplastic epidermis alterations were observed after UVB exposure of vehicle-applied mouse skin (Figure 4A vs. B). By contrast, the alterations in the TiO_2 and 100-nm ND groups were much milder (Figure 4C and D vs. B; 4I, quantified results). The number of infiltrated leukocytes in the dermis was significantly higher in vehicle-treated groups than in the control groups (Figure 4E vs. F), clearly indicating an inflammatory response, but not in

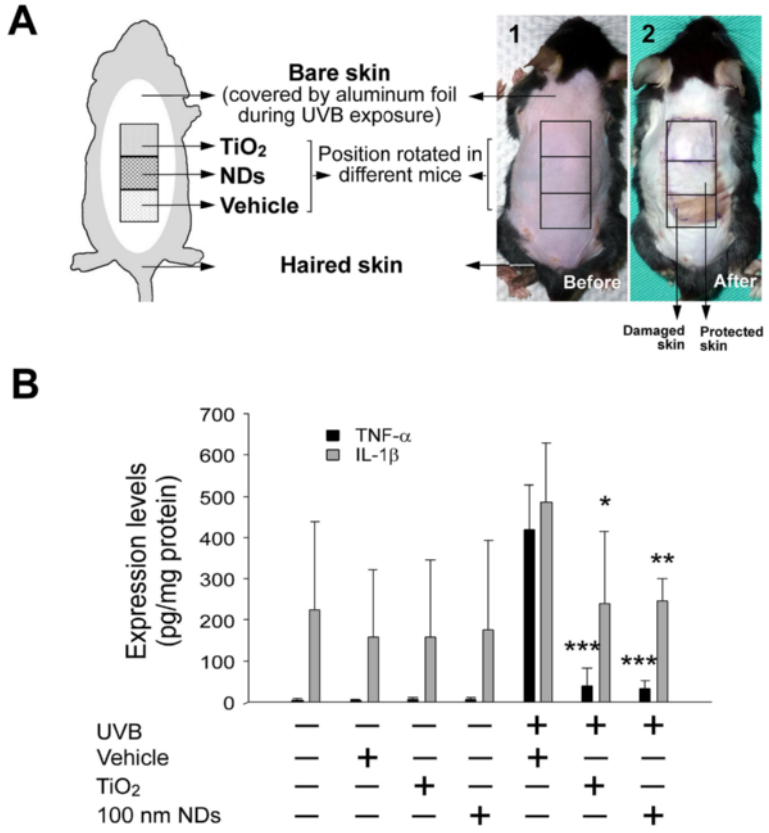

Figure 3 NDs protect C57BL/6J mouse skin from UVB-induced inflammation. Experiment setting **(A)** and the typical appearance of hair-removed mouse skin before (A1) and three days after UVB irradiation [UVI 6, 20 min per day, 3 cycles; (135.9 mJ/cm^2/day × 3 days)], with or without protection at 2 mg/cm^2 nanomaterial density (A2). Bare skin surrounding the experimental area was protected using aluminum foil. Each material was applied to the anterior, middle, and posterior position three times on three mice **(A)**. TNF-α and IL-1β in mouse skin are reported as pg per mg of protein **(B)**. n = 9 (three experiments repeated three times). *P < 0.05, **P < 0.01, ***P < 0.001; significant amelioration versus respective UVB vehicle groups. Data are mean ± SD.

the nanosized TiO_2 and 100-nm ND groups (Figure 4G and H vs. F; J, quantified results).

Detections of 100-nm NDs on UVB-irradiated mouse skin and ND emission spectra

NDs are biocompatible materials [32]. However, their long-term effects remain unclear, and their accumulation and retention in the body should be avoided. To investigate whether 100-nm NDs can penetrate through the skin, particularly after sunburns, the skin of experimental mice were examined. We found 100-nm NDs only in the stratum granulosum and not in the deeper layers, even after intensive UVB irradiation (Figure 5). The epidermis, including the stratum granulosum, is gradually replacing by newly produced cells, and these NDs should theoretically along with the dead skin cells. Notably, on excitation with 266 nm UV, 5-nm but not 100-nm NDs displayed a unique emission pattern at approximately 320–400 nm in the UVA range (Figure 6A), which is harmful to the skin.

Furthermore, 100-nm but not 5-nm NDs elicited higher emissions in the infrared range on excitation with both 266- and 325-nm UV (Figure 6; 800–900-nm infrared). More UV energy can be transformed into relatively noncytotoxic infrared energy without eliciting harmful UVA, and this is likely part of the mechanism underlying 100-nm NDs exhibiting superior UV protection compared with 5-nm NDs (Figure 2C, 20-min group). These results collectively suggested that 100-nm NDs are a suitable sunscreen material.

Discussion

UV-induced skin damage, such as acute sunburn, photoaging, and skin cancers, have been widely investigated through cell, animal, and human studies. However, few studies have studied the potential of NDs as UV filters. Our study found that NDs can attenuate UVB intensity, increase HaCaT and MEF cell viability, and ameliorate inflammatory responses of C57BL/6J mouse skin under UVB exposure. Moreover, their efficiency was comparable

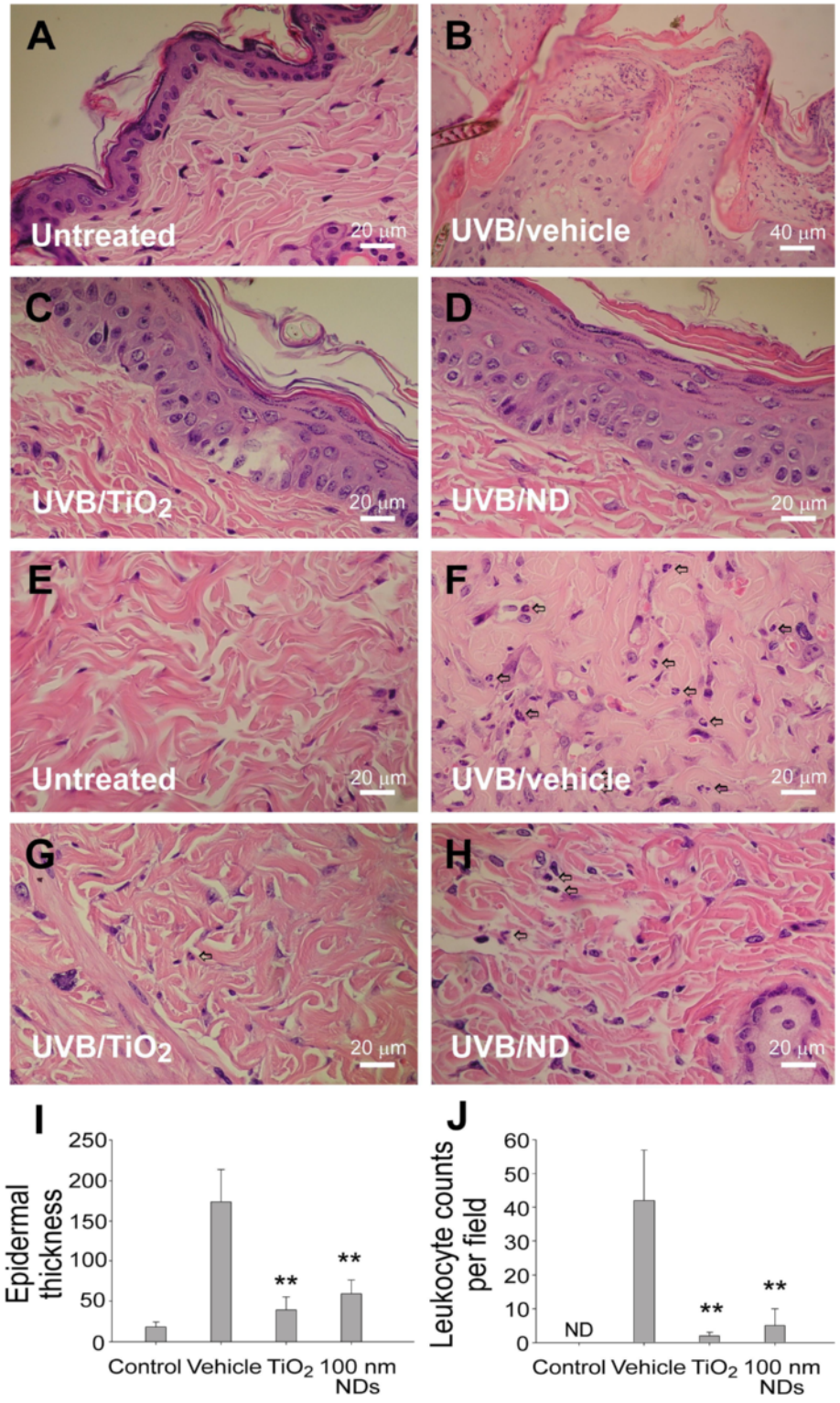

Figure 4 NDs ameliorate UVB-induced skin hyperplasia and leukocyte infiltration. Histological examinations of the epidermis **(A–D)** and dermis **(E–H)** revealed the alterations before **(A, E)** and 3 days after UVB irradiation [UVI 6, 20 min per day, three cycles; (135.9 mJ/cm^2/day × 3 days)], with and without protection using 2 mg/cm^2 TiO_2 and 100-nm ND nanomaterials (**B–D, F–H;** H&E stain, × 400, scale bars in A and C–H = 20 μm and in B = 40 μm). The epidermal thickness was quantified as indicated **(I)**. The infiltrated leukocytes (indicated by arrows) were found in the dermis, especially in the vehicle group **(F–H)**; quantified results are presented in **(J)**. n = 9, $^{**}P < 0.01$, significant amelioration versus vehicle groups. Data are mean ± SD.

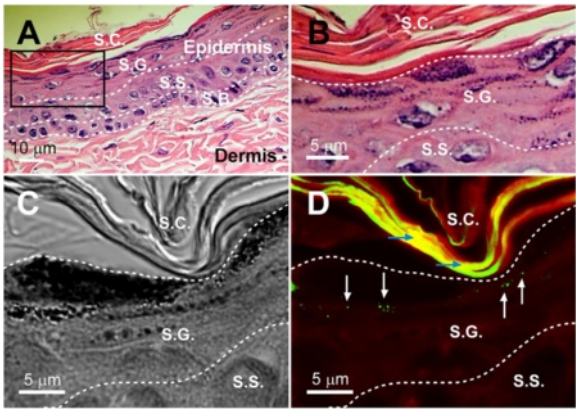

Figure 5 Detecting 100-nm NDs on UVB-irradiated mouse skin. An H&E-stained mouse skin section was used as a sample to illustrate the relative positions and morphology of the epidermis, dermis **(A)**, stratum corneum, and stratum granulosum (S.G.) **(B)**. The area indicated by the black box in **(A)** is magnified in **(B)**. Differential interference contrast **(C)** and confocal microscopy **(D)** images of a 100-nm-ND-shielded UVB-irradiated mouse skin. Dosages of UVB irradiation and 100-nm NDs are the same as those in Figure 4. White arrows indicate the fluorescent signals (501–511 nm; green labels) emitted by the 100-nm NDs, which did not penetrate beyond the S.G. **(D)**. Stratum corneum (S.C.), S.G., stratum spinosum (S.S.), and stratum basale (S.B.) are indicated. Blue arrows indicate keratin autofluorescence.

with those of nanosized TiO_2 and ZnO, which are currently extensively utilized in sunscreens.

Irradiance (in W/cm^2) is usually used to express UV intensity [1]. However, because the deleterious effects of UV are associated with UV wavelength, irradiance cannot reflect the true damaging ability. Erythemally weighted UV radiation (UV_{Ery}) calculated according to the erythema reference action spectrum of the International Commission of Illumination more accurately estimates the harmful effects of UV on the skin [33]. This study adopted the UVI because it is based on UV_{Ery} and is the standard of UV reporting recommended by WHO, making our results applicable to everyday life [6]. Minimal erythema dose (MED) is another common measure of UV radiation [34,35]. However, because of the variance in individual sensitivity to UV radiation, MED is more appropriate for observational studies [1,36].

According to the regulations of the Food and Drug Administration of the United States, the sun protection factor of sunscreen ingredients are determined at a concentration of 2 mg/cm^2 [37]. Therefore, we adopted the same concentration in our animal study. However, because most people apply insufficient sunscreen amounts, we further examined the protective ability of NDs at lower concentrations in UVB attenuation and cell viability tests.

Keratinocytes are a major cell type used in UV-related experiments because they are a major component of the epidermis, the outmost skin layer directly absorbing UV irradiation [15,38]. NDs, nanosized TiO_2, and ZnO successfully attenuated extreme UVB (UVI = 11) to safe levels (UVI < 2). Additionally, these nanomaterials, particularly the 100-nm NDs, efficiently protected human HaCaT keratinocytes at 1 mg/cm^2. Apart from keratinocytes, we used fibroblasts for *in vitro* analysis for the following three reasons. First, fibroblasts are the main cell type in the dermis, which constitutes a large percentage of the skin. UV with longer wavelengths penetrates deep into the dermal layer. Second, the UV-induced photodamage response and signaling pathways in humans and mice are not identical. Cutaneous IL-1β after UV irradiation arises from keratinocytes in humans but from infiltrating bone marrow-derived cells and Langerhans cells in mice [39]. Third, dermal fibroblasts are involved in photoaging and skin cancer [40,41]. Although MEFs are more sensitive to UVB irradiation than HaCaT cells, all the aforementioned nanomaterials efficiently protect MEFs at 2 mg/cm^2.

Animal models are useful and essential in UV-induced skin damage studies. Because hairless mice develop squamous cell carcinoma after chronic UV exposure and

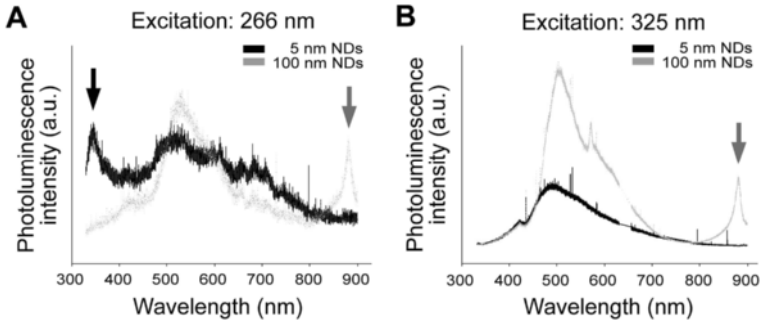

Figure 6 Photoluminescence of NDs. The photoluminescence properties of 5 and 100-nm NDs were characterized under excitation by 266 nm **(A)** and 325 nm UV **(B)** (i.e., the wavelengths approximately at the edges of UVB range), respectively. Gray arrows indicate the unique emission patterns of 100-nm NDs in the 800–900-nm (infrared) range **(A, B)**. A black arrow indicates the unique emission pattern of 5-nm NDs in the 320–400-nm (UVA) range **(A)**.

support easy manipulation and skin observations [42], they have been widely utilized in skin-related research, especially SKH-1 mice [43,44]. We examined C57BL/6J mice because a previous study compared three strains of mice, C57BL/6J, SKH-1, and Balb/c, and concluded that C57BL/6J mice were the most similar to humans in photodamage, including in thickening of the epidermis, infiltration of inflammatory cells in the dermis, induction of TNF-α mRNA, and accumulation of glycosaminoglycans [45], whereas hairless SKH-1 mice lacked TNF-α mRNA induction. The histological findings were the same as those in the previous report, and a TNF-α assay correlated well with gross skin damage. Therefore, the C57BL/6J mouse model used in this study is effective for evaluating UV-induced injury.

The mechanism of nanosized TiO_2 as a UV filter, which depends mainly on reflection, scattering, and absorption, has been studied extensively [9,46]. By contrast, ND–UV interaction has received little attention. The nitrogen-vacancy center in NDs absorbs strongly at approximately 560 nm and fluoresces efficiently at approximately 700 nm [47]. Moreover, ND optical properties can be altered through surface modification. For example, NDs covalently attached with octadecylamine emit bright blue light when irradiated with UV light [16]. Additionally, in this study, on excitation with UVB, 100-nm NDs elicited emissions not only in the visible-light range but also in the infrared range (Figure 6; 800–900 nm). These evidences collectively suggest that in addition to UVB shielding and scattering, NDs attenuate UVB energy by transformation it to safe visible and infrared light.

UV attenuation of nanomaterials depends largely on particle size. Primary nanosized TiO_2 and ZnO particles cluster and form tightly bound aggregates with sizes between 30 and 150 nm. Subsequently, the aggregates loosen to form agglomerates with sizes over 1 μm. Nanosized TiO_2 with an average size of 100 nm efficiently blocks both UVA and UVB. At an average size of 50 nm, UVB attenuation increases but UVA attenuation decreases. On reducing the average size to 20 nm, nanosized TiO_2 offers significantly lower protection against both UVA and UVB [10]. Smaller, stabilized, and nonagglomerated TiO_2 nanoparticles have superior UV attenuation [48]. NDs of various particle sizes have been studied and 100 nm NDs were suggested to be potentially useful in sunscreen formulations because of visual transparency and remarkable UVA, UVB, and UVC shielding [17].

Conclusions

This study demonstrated for the first time that NDs attenuate UVB and efficiently protect keratinocytes, fibroblasts, and C57BL/6J mouse skin from UVB-induced damage. The 100-nm NDs exhibit superior UVB attenuation compared with nanosized TiO_2, ZnO, and 5-nm NDs in the HaCaT keratinocyte model, and both 5 and 100-nm NDs exhibit superior UVB attenuation compared with nanosized ZnO in the MEF model. The protective efficiency of 100-nm NDs is comparable to that of nanosized rutile TiO_2 in the animal model. Additionally, NDs are safe materials without considering the elicitation of ROS during UV irradiation. These results collectively suggest that NDs can be a "diamond-class" sunscreen ingredient.

Methods

UV related equipment and nanomaterials

UVB radiation was generated using a UVB lamp (G25T8E, Sankyo Denki Co., Kanagawa, Japan) with peak emission at 306 nm. UV intensity, reported as the UVI, was measured using a UVI meter (ARCS Precision Co., Taichung, Taiwan). Using previously reported methods [33,35], the conversion of UV-irradiation dose versus the UVI is as follows: 1 UVI = 25 mW/m^2 UV_{Ery} (erythemally weighted UV radiation). Irradiation at a UVI of 6 for 20 min, used in our mouse experiments, were equivalent to 6×25 mW/m^2 $UV_{Ery} \times 1200$ s (=180 J/m^2 UV_{Ery}; = 1359 J/m^2 UVB; = 135.9 mJ/cm^2; = 3.775 MED; for B6 mice, 1 MED = 36 mJ/cm^2 [35]). Rutile nanosized TiO_2 was purchased from Advanced Ceramics Nanotech Co., Ltd (Tainan, Taiwan). A UV cut-off filter was fabricated by depositing the nanomaterials on a commercial food wrap film. A lubricating jelly (PDI, Orangeburg, NY, USA) composed of water and glycerin served as the vehicle for mixing the nanomaterials; it facilitated even dispersion of nanomaterials and its adherence to the film and skin.

MEF and HaCaT keratinocyte cell cultures

MEFs were obtained using previously described methods [49,50]. Human immortalized HaCaT keratinocytes were maintained using previously described methods [51]. After thawing the frozen MEF and HaCaT cells, they were cultured with Dulbecco's modified Eagle's medium (DMEM) containing 10% fetal bovine serum (FBS), L-glutamine, and penicillin–streptomycin and grown in a 37°C, 5% CO_2 incubator. The medium was changed after the first day and every two days thereafter. On confluence, the cells were trypsinized for passage.

Animal study

Male C57BL/6J mice were purchased from the National Laboratory Animal Center and housed in the Laboratory Animal Center, Tzu-Chi University, until they were 8–9 weeks old. The hair on the backs of the mice was removed using commercial hair removal creams containing thioglycolate trihydrate (approximately 250 μL/mouse) 2–3 days before the experiments. The mice underwent the procedures under anesthesia with an intraperitoneal injection of ketamine : xylazine (80 : 10 mg/kg body weight). The

research methods were approved by the Animal Care and Use Committee of Tzu-Chi University (approval ID 99047).

Measurement of UV attenuation by nanoparticle-coated films

The attenuation efficiencies of four nanomaterials—5-nm NDs, 10-nm NDs, nanosized rutile TiO_2, and ZnO—in attenuating UV radiation were tested. Each nanomaterial was mixed thoroughly with the vehicle (lubricating jelly) and applied to a thin plastic film at concentration of 1, 2, and 3 mg/cm^2 for use as a UV filter. The UV intensity was measured using a UVI meter, and UVB at UVIs of 4, 6, 9, and 11, which respectively correspond to moderate, high, very high, and extreme exposure categories, were determined. The degree of attenuation was determined by comparing the UVI values with and without the UV filters.

MB degradation

MB analyses for analyzing photocatalytic performance of TiO_2 were conducted according to previously reported methods [52-54]. Photocatalytic efficiency was measured through the decomposition of 100 ppm (0.1 mg/mL) MB (Koch-Light Laboratories, Colnbrook, Bucks., England) at a nanomaterial concentration of 1.5 mg/mL. MB concentration intensity was monitored in the light absorption peak at a 663-nm wavelength by using a UV–Vis spectrometer. UV irradiation was performed using a UVB lamp (G25T8E, Sankyo Denki) with an average power density of 150 mW/m^2 UV_{Ery} and 15 cm of spacing between the UV source and the sample. Anatase TiO_2 (UV100, Sachtleben, Germany), which exhibits photocatalysis only when irradiated with UV light [24,55], served as the positive control in photocatalytic MB.

Cell viability analyses

We used the cell culture model for evaluating the protective effects of the four nanomaterials. Cultured MEFs were seeded in a 96-well microplate (10^5 cells/well) containing 200 μL/well of DMEM and 10% FBS, and grown in a 37°C, 5% CO_2 incubator. On the second day, the MEFs were irradiated with UVB at a UVI of 6 for 5, 10, and 20 min with and without the UV filter containing 2 mg/cm^2 of each nanomaterial. In addition, the cells were irradiated for 10 min with UV filters containing 1, 2 and 3 mg/cm^2 of the nanomaterials. The culture medium was replaced by no-phenol-red medium during UVB irradiation. On the third day, the cultured cells were water-soluble tetrazolium (WST-1) assayed (Roche Diagnostics GmbH, Mannheim, Germany) [56,57]. The culture medium was removed and 100 μL of WST-1 reagent diluted with RPMI-1640 medium (1:19) was added to each well. After incubating at 37°C for 30 min, the WST-1 solutions were pipetted to a new microplate, and absorbance at 450 nm was measured using an ELISA reader. The cells not subjected to UVB irradiation were considered to have 100% cell survival, and the viability of the other study groups was calculated by comparing the WST-1 assay results.

Cytokine analyses

We established an animal model to examine the efficiency of these nanomaterials in blocking UVB radiation. After irradiating the mice, TNF-α and IL-1β levels in the skin, which represents the degree of injury, were measured using ELISA (BioLegend, San Diego, CA, USA). The bare back skin of the mice was marked with four 1 cm × 1 cm areas on which were applied nothing, vehicle (jelly), 2 mg/cm^2 100-nm NDs, and nanosized TiO_2. The mice were not subjected to UVB irradiation, and these materials were removed after 20 min. This procedure was repeated on three consecutive days. On the fourth day, the mice were sacrificed by CO_2 inhalation and the skins were processed for a cytokine assay. In another group of mice, vehicle (jelly), 2 mg/cm^2 100-nm NDs, and nanosized TiO_2 were applied in three longitudinally adjacent 1 cm × 1 cm areas on the back midline. The bare skin around the experimental area was protected with aluminum foil. The mice were irradiated with UVB at a UVI of 6 for 20 min, after which these materials were removed. This procedure was repeated on three consecutive days. The mice were sacrificed on the fourth day, and skin sections with a diameter of 0.7 cm containing the marked areas were excised for analysis. The skin samples were cut into small pieces and preserved in a 2-mL Eppendorf tube containing 700 μL of phosphate buffered saline (PBS) and 5 mM phenylmethanesulfonyl fluoride (PMSF), which decreased cytokine degradation [58]. The skin samples were homogenized and centrifuged at 4°C and 16,000 × g for 20 min. The supernatant was aspirated for additional quantification analyses of the protein and cytokine concentrations. The samples were placed on ice during processing [59,60].

Enzyme-linked immunosorbent assay

TNF-α and IL-1β were quantified using commercial equipment (ELISA MAX™ Deluxe Sets, BioLegend, San Diego, CA, USA). One day prior to skin sample preparation, 100 μL of capture antibody solution was added to each well of a 96-well microplate and incubated overnight at 4°C. On the second day, after irradiation blocking, the solution was discarded and the microplate washed three times with 200 μL of PBS containing 0.05% Tween-20 per well. Two hundred microliters of assay diluent was added to the wells and then incubated at 37°C for 2 h. The microplate was washed again three

times; and 100 μL/well solutions of serially diluted standards or processed skin samples were added to each well and then incubated overnight at 4°C. On the third day, the plate was washed three times and incubated at 37°C for 1 h after adding 100 μL of detection antibody to each well. Subsequently, 100 μL of avidin-horseradish peroxidase solution was added to each well and incubated at 37°C for 30 min. The plate was washed, 100 μL of tetramethylbenzidine substrate solution added to each well, and incubated at 37°C for 15 min. The reaction was stopped by adding 50 μL of 2 N hydrogen chloride solution to each well. Absorbance was measured at 450 nm by using an ELISA reader, and the standard curve was generated with a software program by using a four-parameter logistics curve-fitting algorithm. The cytokine levels in the skin samples were calculated from the standard curve. Because the UVB-damaged skin shrank and the skin sample may have been damaged during homogenization, the cytokine levels were normalized to the protein content for comparison. Dye reagent concentrate (Bio-Rad Laboratories, Hercules, CA, USA) was prepared by diluting (1:4) with distilled, deionized water. Bovine serum albumin with concentrations of 2, 1, 0.5, and 0.25 mg/mL were prepared and used as the protein standard. After thoroughly mixing 10 μL of each standard and sample solution with 190 μL of diluted dye reagent and incubating at room temperature for 5 min, the absorbance at 595 nm was measured using an ELISA reader.

Histology examination

After the mice were sacrificed, the skin tissues were cut into three strips, preserved in 4% formaldehyde solution, dehydrated, and embedded in paraffin wax. Tissue sectioning and hematoxylin-eosin (H&E) staining were performed according to previously reported methods [57]. Thickness from the stratum granulosum to the stratum basale and neutrophil content within the dermis were measured at three random sites on each tissue strip.

Confocal microscopy

Skin-tissue sections were obtained using protocols described in the aforementioned histology examinations. Fluorescence images of the skin sections were obtained using a confocal laser-scanning fluorescence microscope (TCS SP5, Leica, Germany; 63 × oil immersion). UV (405 nm) and argon lasers (458/476/488/514 nm) were employed for analyzing ND distribution in skin sections. ND fluorescence signals were excited at 405 nm and the resulting emissions were collected at 501–511 nm, as shown in green in Figure 5D. The fluorescence signals of the skin sections were excited at 488 nm and the resulting emissions were collected at 498–584 nm, as showed in red in Figure 5D.

Photoluminescence

Different sizes of NDs (5- and 10-nm; Kay Diamond, USA) were used. For characterization, the obtained nanoparticle powders (NPs) was separately dispersed in deionized water at a concentration of 2 mg/mL. From each suspension, 20 μL was dropped onto a single crystal Si (100) wafer and dried. Photoluminescence (PL) of NPs were measured using a confocal microspectrometer (Jobin Yvon, T64000, France) equipped with a 325-nm liquid-N_2 cooled charge-coupled detector (He–Cd gas phase laser, Kimmon Koha, Japan). The laser power supplied through the objective lens was estimated to be 20 mW (325-nm excitation, measured from the laser output). For macro-PL spectrometer (Horiba, HR-550, Japan) with a laser excitation wavelength of 266 nm (Nd–YAG, Laser-Export, USA), the laser power was 2 mW.

Statistical analyses

The experimental results were analyzed using Microsoft Office Excel 2003 and SPSS 17, and the results reported as mean ± standard deviation (SD). Statistical significance of the obtained results was examined using a one-way analysis of variance the probability of type 1 error $\alpha = 0.05$ was considered the threshold of statistical significance.

Supporting information

Supporting information is available online.

Additional files

Additional file 1: Figure S1. Relative UVB attenuation ability of tested materials. **Figure S2**. UVB illumination on mouse embryonic fibroblasts. **Figure S3**. Methylene blue degradation experiment. **Figure S4**. UVB-induced skin inflammation. **Figure S5**. Dye exclusion experiment.

Abbreviations

UV: Ultraviolet; NDs: Nanodiamonds; WHO: World Health Organization; UVI: UV index; TiO_2: Titanium dioxide; ZnO: Zinc oxide; ROS: Reactive oxygen species; NPs: Nanoparticles; MEFs: Mouse embryonic fibroblasts; ELISA: Enzyme-linked immunosorbent assay; TNF-α: Tumor necrosis factor-α; IL-1β: Interleukin-1β; UV_{Ery}: Erythemally weighted UV radiation; CIE: International Commission of Illumination (usually abbreviated CIE for its French name, Commission internationale de l'éclairage); MED: Minimal erythema dose; DMEM: Dulbecco's modified Eagle's medium; FBS: Fetal bovine serum; WST-1: Water soluble tetrazolium; PBS: Phosphate buffered saline; PMSF: Phenylmethanesulfonyl fluoride; HRP: Horseradish peroxidase; TMB: Tetramethylbenzidine; HCl: Hydrogen chloride; H&E: hematoxylin-eosin; SD: Standard deviation; ANOVA: Analysis of variance..

Competing interests

The authors declare that they have no competing interests.

Authors' contributions

Conceived and designed the experiments: MSW, DSS, HHC. Performed the experiments: MSW, YCL, SCH. Analyzed the data: MSW, YCL, HHC. Contributed reagents/materials/analysis tools: CLC, PKC, JHY. Wrote the paper: MSW, HHC. All authors read and approved the final manuscript.

Acknowledgements
This work was supported by Tzu-Chi University under grant numbers: TCIRP101001 and TCRPP103001, and Ministry of Science and Technology R.O.C. under grant number: 102-2120-M-259 -001.

Author details
[1]Division of Plastic Surgery, Department of Surgery, Buddhist Tzu Chi General Hospital, No. 707 Sec. 3, Chung-Yang Rd, Hualien City, Hualien County 970, Taiwan. [2]Department of Molecular Biology and Human Genetics, Tzu-Chi University, No. 701 Sec. 3, Chung-Yang Rd, Hualien City, Hualien County 970, Taiwan. [3]Research Center of Nanobiomedical Science, Tzu-Chi University, No. 701 Sec. 3, Chung-Yang Rd, Hualien City, Hualien County 970, Taiwan. [4]Department of Physics, National Dong Hwa University, No. 1 Sec. 2, University Road, Shoufeng Township, Hualien County 974, Taiwan. [5]Nanotechnology Research Center, National Dong Hwa University, No. 1 Sec. 2, University Road, Shoufeng Township, Hualien County 974, Taiwan. [6]Department of Biochemistry, School of Medicine, Tzu Chi University, No. 701 Sec. 3, Chung-Yang Rd, Hualien City, Hualien County 970, Taiwan. [7]Institute of Medical Sciences, School of Medicine, Tzu Chi University, No. 701 Sec. 3, Chung-Yang Rd, Hualien City, Hualien County 970, Taiwan. [8]Department of Dermatology, Buddhist Tzu Chi General Hospital, No. 707 Sec. 3, Chung-Yang Rd, Hualien City, Hualien County 970, Taiwan.

Received: 11 January 2015 Accepted: 29 April 2015
Published online: 07 May 2015

References

1. Diffey BL. Sources and measurement of ultraviolet radiation. Methods. 2002;28:4–13.
2. Harmful effects of ultraviolet radiation. Council on Scientific Affairs. JAMA 1989, 262:380–384.
3. Balk SJ. Ultraviolet radiation: a hazard to children and adolescents. Pediatrics. 2011;127:e791–817.
4. Matsumura Y, Ananthaswamy HN. Short-term and long-term cellular and molecular events following UV irradiation of skin: implications for molecular medicine. Expert Rev Mol Med. 2002;4:1–22.
5. Farman JC, Gardiner BG, Shanklin JD. Large losses of total ozone in Antarctica reveal seasonal ClOx-NOx interaction. Nature. 1985;315:207–10.
6. WHO. Global Solar UV Index: A Practical Guide. Geneva, Switzerland, World Health Organization; 2002.
7. WHO. INTERSUN: the Global UV Project: a guide and compendium. Geneva, Switzerland, World Health Organization; 2003.
8. Lautenschlager S, Wulf HC, Pittelkow MR. Photoprotection. Lancet. 2007;370:528–37.
9. Burnett ME, Hu JY, Wang SQ. Sunscreens: obtaining adequate photoprotection. Dermatol Ther. 2012;25:244–51.
10. Wang SQ, Tooley IR. Photoprotection in the era of nanotechnology. Semin Cutan Med Surg. 2011;30:210–3.
11. Smijs TG, Pavel S. Titanium dioxide and zinc oxide nanoparticles in sunscreens: focus on their safety and effectiveness. Nanotechnol Sci Appl. 2011;4:95–112.
12. Monteiro-Riviere NA, Wiench K, Landsiedel R, Schulte S, Inman AO, Riviere JE. Safety evaluation of sunscreen formulations containing titanium dioxide and zinc oxide nanoparticles in UVB sunburned skin: an in vitro and in vivo study. Toxicol Sci. 2011;123:264–80.
13. Nohynek GJ, Dufour EK. Nano-sized cosmetic formulations or solid nanoparticles in sunscreens: a risk to human health? Arch Toxicol. 2012;86:1063–75.
14. Newman MD, Stotland M, Ellis JI. The safety of nanosized particles in titanium dioxide- and zinc oxide-based sunscreens. J Am Acad Dermatol. 2009;61:685–92.
15. Yin JJ, Liu J, Ehrenshaft M, Roberts JE, Fu PP, Mason RP, et al. Phototoxicity of nano titanium dioxides in HaCaT keratinocytes–generation of reactive oxygen species and cell damage. Toxicol Appl Pharmacol. 2012;263:81–8.
16. Mochalin VN, Shenderova O, Ho D, Gogotsi Y. The properties and applications of nanodiamonds. Nat Nanotechnol. 2012;7:11–23.
17. Shenderova O, Grichko V, Hens S, Walch J. Detonation nanodiamonds as UV radiation filter. Diam Relat Mater. 2007;16:2003–8.
18. Liou JW, Chang HH. Bactericidal effects and mechanisms of visible light-responsive titanium dioxide photocatalysts on pathogenic bacteria. Arch Immunol Ther Exp (Warsz). 2012;60:267–75.
19. Yin B, Zhang S, Zhang D, Jiao Y, Liu Y, Qu F, et al. ZnO Film Photocatalysts. J Nanomaterials 2014; 2014:ID 186916.
20. Hashimoto K, Irie H, Fujishima A. TiO2 Photocatalysis: A Historical Overview and Future Prospects. Jpn J Appl Phys. 2005;44:8269–85.
21. Tseng YH, Sun DS, Wu WS, Chan H, Syue MS, Ho HC, et al. Antibacterial performance of nanoscaled visible-light responsive platinum-containing titania photocatalyst in vitro and in vivo. Biochim Biophys Acta. 1830;2013:3787–95.
22. Chang WK, Sun DS, Chan H, Huang PT, Wu WS, Lin CH, et al. Visible light-responsive core-shell structured In_2O_3@$CaIn_2O_4$ photocatalyst with superior bactericidal properties and biocompatibility. Nanomedicine. 2012;8:609–17.
23. Wong MS, Chu WC, Sun DS, Huang HS, Chen JH, Tsai PJ, et al. Visible-light-induced bactericidal activity of a nitrogen-doped titanium photocatalyst against human pathogens. Appl Environ Microbiol. 2006;72:6111–6.
24. Liou JW, Gu MH, Chen YK, Chen WY, Chen YC, Tseng YH, et al. Visible light responsive photocatalyst induces progressive and apical-terminus preferential damages on Escherichia coli surfaces. PLoS One. 2011;6:e19982.
25. Chen YL, Chen YS, Chan H, Tseng YH, Yang SR, Tsai HY, et al. The use of nanoscale visible light-responsive photocatalyst TiO2-Pt for the elimination of soil-borne pathogens. PLoS One. 2012;7:e31212.
26. Wong MS, Sun DS, Chang HH. Bactericidal performance of visible-light responsive titania photocatalyst with silver nanostructures. PLoS One. 2010;5:e10394.
27. Kau JH, Sun DS, Huang HH, Wong MS, Lin HC, Chang HH. Role of visible light-activated photocatalyst on the reduction of anthrax spore-induced mortality in mice. PLoS One. 2009;4:e4167.
28. Segre JA, Bauer C, Fuchs E. Klf4 is a transcription factor required for establishing the barrier function of the skin. Nat Genet. 1999;22:356–60.
29. Hardman MJ, Sisi P, Banbury DN, Byrne C. Patterned acquisition of skin barrier function during development. Development. 1998;125:1541–52.
30. Yano K, Kadoya K, Kajiya K, Hong YK, Detmar M. Ultraviolet B irradiation of human skin induces an angiogenic switch that is mediated by upregulation of vascular endothelial growth factor and by downregulation of thrombospondin-1. Br J Dermatol. 2005;152:115–21.
31. Imokawa G. Mechanism of UVB-induced wrinkling of the skin: paracrine cytokine linkage between keratinocytes and fibroblasts leading to the stimulation of elastase. J Investig Dermatol Symp Proc. 2009;14:36–43.
32. Zhu Y, Li J, Li W, Zhang Y, Yang X, Chen N, et al. The biocompatibility of nanodiamonds and their application in drug delivery systems. Theranostics. 2012;2:302–12.
33. McKenzie R, Smale D, Kotkamp M. Relationship between UVB and erythemally weighted radiation. Photochem Photobiol Sci. 2004;3:252–6.
34. Goettsch W, Garssen J, de Gruijl FR, Dortant P, van Loveren H. Methods for exposure of laboratory animals to ultraviolet radiation. Lab Anim. 1999;33:58–67.
35. Sumiyoshi M, Kimura Y. Effects of olive leaf extract and its main component oleuroepin on acute ultraviolet B irradiation-induced skin changes in C57BL/6J mice. Phytother Res. 2010;24:995–1003.
36. Chang CP, Liu HH, Peng CY, Fang HY, Tsao TH, Lan CH. Evaluation of erythemal UV effective irradiance from UV lamp exposure and the application in shield metal arc welding processing. Health Phys. 2008;94:318–27.
37. FDA: Sunscreen Drug Products for Over-the-Counter Human Use; Final Rules and Proposed Rules. In: Federal Register, vol. 76. pp. 35620–35665. Silver Spring, MD, USA, Food and Drug Administration, Department of Health and Human Services; 2011.
38. Bernard JJ, Cowing-Zitron C, Nakatsuji T, Muehleisen B, Muto J, Borkowski AW, et al. Ultraviolet radiation damages self noncoding RNA and is detected by TLR3. Nat Med. 2012;18:1286–90.
39. Nasti TH, Timares L. Inflammasome activation of IL-1 family mediators in response to cutaneous photodamage. Photochem Photobiol. 2012;88:1111–25.
40. Polefka TG, Meyer TA, Agin PP, Bianchini RJ. Effects of solar radiation on the skin. J Cosmet Dermatol. 2012;11:134–43.
41. Tulah AS, Birch-Machin MA. Stressed out mitochondria: the role of mitochondria in ageing and cancer focussing on strategies and opportunities in human skin. Mitochondrion. 2013;13:444–53.
42. Winkelmann RK, Baldes EJ, Zollman PE. Squamous cell tumors induced in hairless mice with ultraviolet light. J Invest Dermatol. 1960;34:131–8.
43. Bae JY, Choi JS, Kang SW, Lee YJ, Park J, Kang YH. Dietary compound ellagic acid alleviates skin wrinkle and inflammation induced by UV-B irradiation. Exp Dermatol. 2010;19:e182–90.

44. Kligman LH. The hairless mouse model for photoaging. Clin Dermatol. 1996;14:183–95.
45. Sharma MR, Werth B, Werth VP. Animal models of acute photodamage: comparisons of anatomic, cellular and molecular responses in C57BL/6J, SKH1 and Balb/c mice. Photochem Photobiol. 2011;87:690–8.
46. Murphy GM. Sunblocks: mechanisms of action. Photodermatol Photoimmunol Photomed. 1999;15:34–6.
47. Yu SJ, Kang MW, Chang HC, Chen KM, Yu YC. Bright fluorescent nanodiamonds: no photobleaching and low cytotoxicity. J Am Chem Soc. 2005;127:17604–5.
48. Tyner KM, Wokovich AM, Godar DE, Doub WH, Sadrieh N. The state of nano-sized titanium dioxide (TiO2) may affect sunscreen performance. Int J Cosmet Sci. 2011;33:234–44.
49. Jozefczuk J, Drews K, Adjaye J: Preparation of mouse embryonic fibroblast cells suitable for culturing human embryonic and induced pluripotent stem cells. J Vis Exp;64:2012.
50. Conner DA: Mouse embryo fibroblast (MEF) feeder cell preparation. In: Ausubel FM, Brent R, Kingston RE, Moore DD, Seidman JG, Smith JA, Struhl K, editors. Curr Protoc Mol Biol. New York, Wiley; 2001. Unit 23.2:1-7.
51. Ying TH, Chen CW, Hsiao YP, Hung SJ, Chung JG, Yang JH. Citric acid induces cell-cycle arrest and apoptosis of human immortalized keratinocyte cell line (HaCaT) via caspase- and mitochondrial-dependent signaling pathways. Anticancer Res. 2013;33:4411–20.
52. Asahi R, Morikawa T, Ohwaki T, Aoki K, Taga Y. Visible-light photocatalysis in nitrogen-doped titanium oxides. Science. 2001;293:269–71.
53. Lin WL L, Zhu YX, Zhao BY, Xie YC, He Y, Zhu YF. Uniform carbon-covered titania and its photocatalytic property. J Mol Catal A Chem. 2005;236:46–53.
54. Zhang H, Zong R, Zhao J, Zhu Y. Dramatic visible photocatalytic degradation performances due to synergetic effect of TiO2 with PANI. Environ Sci Technol. 2008;42:3803–7.
55. Cheng CL, Sun DS, Chu WC, Tseng YH, Ho HC, Wang JB, et al. The effects of the bacterial interaction with visible-light responsive titania photocatalyst on the bactericidal performance. J Biomed Sci. 2009;16:7.
56. Chang HH, Shyu HF, Wang YM, Sun DS, Shyu RH, Tang SS, et al. Facilitation of cell adhesion by immobilized dengue viral nonstructural protein 1 (NS1): arginine-glycine-aspartic acid structural mimicry within the dengue viral NS1 antigen. J Infect Dis. 2002;186:743–51.
57. Kau JH, Shih YL, Lien TS, Lee CC, Huang HH, Lin HC, et al. Activated protein C ameliorates Bacillus anthracis lethal toxin-induced lethal pathogenesis in rats. J Biomed Sci. 2012;19:98.
58. Jin XJ, Kim EJ, Oh IK, Kim YK, Park CH, Chung JH. Prevention of UV-induced skin damages by 11,14,17-eicosatrienoic acid in hairless mice in vivo. J Korean Med Sci. 2010;25:930–7.
59. Filip A, Clichici S, Daicoviciu D, Catoi C, Bolfa P, Postescu ID, et al. Chemopreventive effects of Calluna vulgaris and Vitis vinifera extracts on UVB-induced skin damage in SKH-1 hairless mice. J Physiol Pharmacol. 2011;62:385–92.
60. Osborne-Hereford AV, Rogers SW, Gahring LC. Neuronal nicotinic alpha7 receptors modulate inflammatory cytokine production in the skin following ultraviolet radiation. J Neuroimmunol. 2008;193:130–9.